Molecular-frame (e,2e) experiment for N_2 at large momentum transfer

D. B. Jones,* M. Yamazaki, N. Watanabe, and M. Takahashi†

Institute of Multidisciplinary Research for Advanced Materials, Tohoku University, Sendai 980-8577, Japan

(Received 15 December 2012; published 27 February 2013)

We report molecular-frame (e,2e) cross sections for N_2 at large momentum transfer, obtained using the electron-electron-fragment ion triple-coincidence technique. The measured angular distribution of the (e,2e) cross section for the inner-valence $2\sigma_g$ orbital appears to show that the spatial character of the orbital has been directly observed in momentum space. On the other hand, experimental results for ionization to states above the double-ionization threshold suggested a larger intensity in the direction perpendicular to the molecular axis rather than parallel, an observation that our plane-wave impulse-approximation calculations fail to reproduce.

DOI: 10.1103/PhysRevA.87.022714 PACS number(s): 34.80.Gs, 34.80.Ht

I. INTRODUCTION

Electron momentum spectroscopy (EMS), or (e,2e) spectroscopy at large momentum transfer, has become a powerful tool for studying the electronic structure of matter [1–6]. Of particular note is its unique ability to look at electron orbitals in momentum space. Within the plane-wave impulse approximation (PWIA) [1–6], the EMS cross section is directly proportional to the product of a spectroscopic factor S_i^f and the spherical average of the square of the normalized momentum space target-ion overlap or Dyson orbital $\psi_i(\boldsymbol{p})$,

$$\sigma_{\mathrm{EMS}}(\boldsymbol{p}) \propto S_i^f \int d\Omega\, |\psi_i(\boldsymbol{p})|^2 . \tag{1}$$

EMS studies on molecules have, however, long been restricted to studying targets with a random spatial orientation. Here spatial information is lost as the orbital densities $|\psi_i(\boldsymbol{p})|^2$ are spherically averaged to obtain one-dimensional momentum distributions $\int d\Omega |\psi_i(\boldsymbol{p})|^2$. Takahashi *et al.* have recently demonstrated that these experimental difficulties could be overcome by measuring the three-dimensional form of molecular orbitals for transitions to the $2s\sigma_g$ and $2p\sigma_u$ excited ion states of H_2 [7–9].

Here a fragment ion, produced through a dissociation process of the residual ion, is also detected in triple coincidence with the two outgoing electrons. To determine the molecular orientation, these measurements rely on the axial-recoil approximation [10]. This approximation states that when the residual ion dissociates much faster than it rotates, the direction of the departing fragment ion coincides with the molecular orientation at the time of ionization. The first (e,2e) experiments using axial-recoil fragmentation processes [7–9], known as molecular-frame (e,2e) spectroscopy, or (e,2e + M) spectroscopy, should therefore be recognized as pioneering work that has opened the door for a detailed analysis of not only the three-dimensional form of molecular orbitals but also stereodynamics in electron-impact ionization of molecules. Indeed, several excellent experiments have subsequently been reported, which have explored the molecular-orientation dependence of (e,2e) cross sections for H_2 [11–14] and N_2 [15,16] at low incident electron energies. With rich structures found in photoelectron angular distributions of fixed-in-space N_2 molecules [17,18], validating the axial-recoil approximation, the work of Takahashi *et al.* [7–9] on H_2 at large momentum transfer can now be extended to N_2.

In this paper, we report on a molecular-frame (e,2e) spectroscopy experiment for N_2 at large momentum transfer. The measured molecular-frame (e,2e) cross sections for the $2\sigma_g$ orbital show that its spatial character has been directly observed in momentum space. On the other hand, experimental results for ionization to states above the double-ionization threshold suggested a larger intensity in the direction perpendicular to the molecular axis rather than parallel, an observation that our PWIA calculations fail to reproduce.

The structure of our paper is as follows. In the next section, our experimental and computational details are discussed. This is followed by the presentation and discussion of our results. Last, conclusions from this work are drawn.

II. EXPERIMENTAL METHOD AND COMPUTATIONAL DETAILS

The present molecular-frame (e,2e) experiment considers the electron-impact ionization of N_2, where two outgoing electrons and a N^+ fragment ion are detected in triple coincidence. The binding energy E_{bind} of the target electron and the recoil momentum of the residual ion $\boldsymbol{q}$, before dissociation of $N_2{}^+$, are obtained through the conservation of energy and linear momentum, respectively,

$$E_{\mathrm{bind}} = E_0 - E_1 - E_2, \tag{2}$$

$$\boldsymbol{q} = \boldsymbol{p}_0 - \boldsymbol{p}_1 - \boldsymbol{p}_2. \tag{3}$$

Here E_i's and $\boldsymbol{p}_i$'s ($i = 0, 1, 2$) are the energies and momenta of the incident and two outgoing electrons, respectively. Under the high-energy Bethe ridge conditions, the (e,2e) collision can be described by a collision of two free electrons with the residual ion acting as a spectator. The momentum of the target electron $\boldsymbol{p}$, before ionization, is then equal in magnitude and opposite in sign to $\boldsymbol{q}$:

$$\boldsymbol{p} = -\boldsymbol{q}. \tag{4}$$

*Present address: School of Chemical and Physics Sciences, Flinders University, GPO Box 2100, Adelaide, South Australia 5001, Australia.

†Corresponding author: masahiko@tagen.tohoku.ac.jp

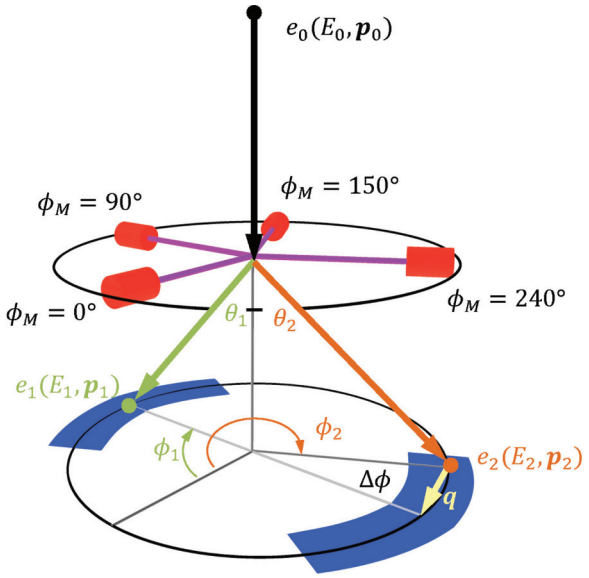

FIG. 1. (Color online) Schematic of the symmetric noncoplanar (e,$2e$ + M) experiment at large momentum transfer.

Further, the orientation of the target N_2 molecules at the time of ionization is determined from the direction of the fragment ion departure. In this way, (e,$2e$) cross sections as a function of E_{bind} and $\boldsymbol{p}$ (or $\boldsymbol{q}$) can be measured with respect to the molecular axis.

The experiment for N_2 has been conducted using our (e,$2e$ + M) spectrometer [7], with the seven ion detectors being replaced by four newly developed detectors. Figure 1 shows a schematic diagram of the experimental setup. Electron-impact ionization occurs when an incident electron ($E_0 = 1230$ eV) collides with a N_2 molecule. Two outgoing electrons, having equal energies ($E_1 = E_2$), emerging at polar angles $\theta_1 = \theta_2 = 45°$ are detected in coincidence. The electrons are selected by a pair of apertures extending over the azimuthal angle ranges of ϕ_1 and ϕ_2 from 70° to 110° and 250° to 290°, respectively. Here, a large acceptance angle has been used to improve the instrumental sensitivity at the expense of the energy ($\Delta E_{\text{bind}} = 7.4$–$8.1$ eV) and momentum ($\Delta q \approx 0.3$ a.u. at $q = 1.0$ a.u.) resolutions. The selected electrons are energy analyzed with a spherical analyzer before being detected with a pair of position-sensitive detectors. Energies and azimuthal angles of the electrons can be determined from their arrival positions at the detectors. On the other hand, N^+ fragment ions have been collected by four detectors using a time-of-flight (TOF) technique. To improve the signal-to-background ratio for (e,$2e$ + M) data, the detectors have been designed and constructed so as to minimize the TOF variation of N^+ fragment ions, which have lower velocities than H^+ fragments detected in our earlier studies [7–9]. Briefly, each detector consisted of an entrance aperture that was located as close as possible to the ionization point. Ions entering the detector experienced a retarding potential that prevented the detection of N_2^+. N^+ fragments, with kinetic energies greater than 0.5 eV, were then detected. The four ion detectors were placed at azimuthal angles ϕ_M's of 0°, 90°, 150°, and 240° in the plane perpendicular to the incident electron beam axis. With this experimental setup, the achieved true triple coincident count rate was ~45 counts per day over the experimental runtime of 124 days.

In the symmetric noncoplanar geometry, the magnitude of the recoil momentum q is solely a function of the out-of-plane azimuthal angle difference between the two outgoing electrons $\Delta\phi$ (=$\phi_2 - \phi_1 - \pi$):

$$q = \sqrt{(p_0 - \sqrt{2}p_1)^2 + [\sqrt{2}p_1 \sin(\Delta\phi/2)]^2}. \quad (5)$$

At high incident electron energy, where $p_0 \approx \sqrt{2}p_1$, the recoil momentum $\boldsymbol{q}$ is dominated by its component perpendicular to $\boldsymbol{p}_0$, i.e., $\boldsymbol{q} \approx \boldsymbol{q}_\perp = \sqrt{2}p_1 \sin(\Delta\phi/2)$. Furthermore, in our experimental setup that covers the ϕ_1 and ϕ_2 ranges, the percentage of $\boldsymbol{q}$'s pointing within ±10° from the $\phi = 0$ or 180° directions is about 74%, and that within ±15° is more than 90% [7,8]. Hence, keeping in mind that the homonuclear target N_2 has inversion symmetry [molecular-frame (e,$2e$) cross section $\sigma(\boldsymbol{q})$ is equal to $\sigma(-\boldsymbol{q})$], the azimuthal angles of the ion detectors (ϕ_M's) approximate the angles made between $\boldsymbol{q}$ and the molecular axis. Thus our experimental setup makes it possible to observe angular distributions of the molecular-frame (e,$2e$) cross section in the case when the molecular axis is perpendicular to $\boldsymbol{p}_0$.

To supplement our experiments, we have calculated molecular-frame (e,$2e$) cross sections within the PWIA. The molecular-frame PWIA cross section is calculated in the same manner as the PWIA cross section [19], except that in the molecular-frame cross section the Dyson orbital is evaluated in the molecular frame, as opposed to undergoing a spherical average. To facilitate the comparison between experiment and PWIA theory, the calculated cross sections are obtained by integrating the PWIA contribution over the range of recoil momenta covered at each ϕ_M angle by the electron detectors. In this way, we obtain molecular-frame cross sections for each ionized orbital under the present experimental configuration. The molecular-frame PWIA cross section for an experimental binding-energy feature is then the summed PWIA contribution for each ionized orbital after being weighted by its spectroscopic intensity in the binding-energy feature. A full discussion of our methods for calculating Dyson orbitals, obtained within a target Kohn-Sham approximation [20,21], and spectroscopic factors is detailed in our earlier publication [19].

III. RESULTS AND DISCUSSION

In Fig. 2 we show a TOF spectrum of N^+ fragment ions, which was created by summing the number of ions arriving at the detector within a small time window when an (e,$2e$) event was observed with a binding energy between 30 and 80 eV. The peak of true triple coincidence events at ~4 μs confirms that successful measurements of vector correlations between the two outgoing electrons and the fragment ion have been achieved here. This peak lies on a flat background produced when (e,$2e$) events were detected with a random ion. The dip at 0 μs corresponds to an inhibit gate applied to the ion signals when the electron signals were collected [7–9].

The triple coincidence events are used to generate the (e,$2e$ + M) binding-energy spectra, presented in Fig. 3. This was accomplished by first obtaining binding-energy spectra, summed over azimuthal angle differences $\Delta\phi$, when ions were

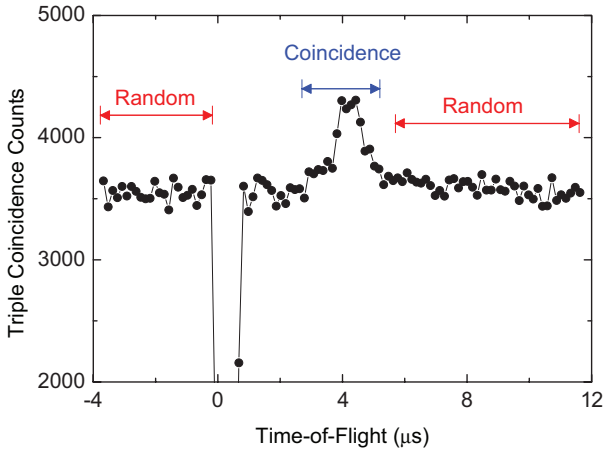

FIG. 2. (Color online) Time-of-flight spectrum of the N^+ fragment ion. The arrows indicate the widths of coincidence and random windows. See text for details.

detected at any ϕ_M angle within the coincidence TOF window (shown in Fig. 2). We then subtracted the (e,2e) binding-energy spectra obtained when random fragment ions were detected, after normalization of the coincidence and random TOF windows, to give the (e,2e + M) spectra. Also shown in Fig. 3 is the traditional (e,2e) binding-energy spectrum [19], which has been normalized to the (e,2e + M) data in the inner-valence region between 30 and 50 eV.

In Fig. 3, we see the expected structure of the (e,2e + M) spectrum. First, the significant spectral contributions from the ionization of the outer-valence $3\sigma_g$, $1\pi_u$, and $2\sigma_u$ orbitals in the (e,2e) spectrum are absent in the (e,2e + M) spectrum. Second, the appearance energy of states that produce N^+ fragment ions is in good accord with the previously determined value of ~27 eV [16]. It is also evident from Fig. 3 that the shapes of the (e,2e + M) and (e,2e) spectra in the inner-valence region are similar to each other. This observation is in accordance with a theoretical prediction [22] which found that all accessible

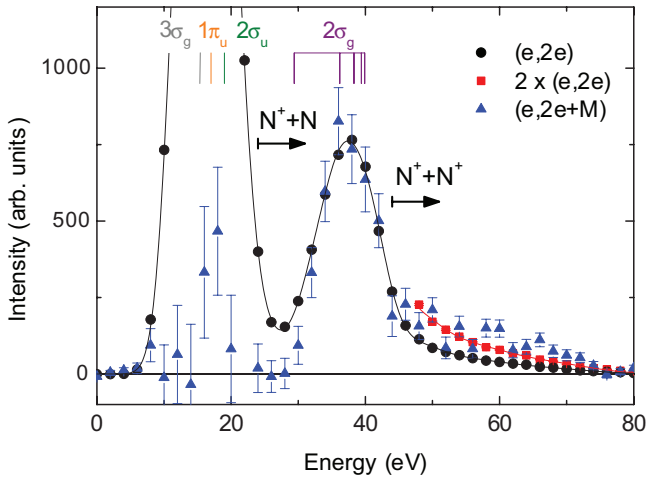

FIG. 3. (Color online) Measured (e,2e) (black circles) and (e,2e + M) (blue triangles) binding-energy spectra of N_2. Also shown is the (e,2e) spectrum scaled by a factor of 2 (red squares). See text for details.

N_2^+ states in this binding-energy range had highly dissociative potential energy curves. Each state contributing to the (e,2e) spectrum should therefore appear in the (e,2e + M) spectrum.

At higher binding energies (E_{bind} > 50 eV), however, one may see that the (e,2e + M) spectrum exhibits a noticeable enhancement over the normalized (e,2e) spectrum. A similar observation has been made in our previous (e,2e + M) experiment on H_2 [7]. For ease of comparison, the present (e,2e) spectrum scaled by a factor of 2 is also given in Fig. 3. It can be seen that the (e,2e + M) spectral intensity is about 2 times larger than the normalized (e,2e) data at binding energies above 50 eV. This observation may be understood by acknowledging that states lying above the double-ionization threshold may converge to $N^+ + N^+$ in the dissociation limit. When two fragment ions are produced from a single (e,2e) event, the probability of observing the (e,2e + M) signal is increased by a factor of 2 compared to cases when an ion and an (undetectable) neutral fragment are produced. Indeed, Auger-electron-ion coincidence [23] and multiphoton double-ionization [24] studies found that $X\,^1\Sigma_g^+$ (E_{bind} = 43.2 eV) and $A\,^1\Pi_u$, $d\,^3\Pi_g$, and $D\,^1\Sigma_u^+$ states (E_{bind} = 45–52 eV) of N_2^{2+} underwent $N_2^{2+} \rightarrow N^+(^3P) + N^+(^3P \text{ or } ^1D)$ dissociation processes with significant kinetic-energy releases. Here N_2^{2+} may be produced through electron-impact double ionization or autoionization of highly excited singly ionized states. In addition, the observed differences for the (e,2e) and (e,2e + M) spectra may arise from (e,2e + M) data being collected only for "side-on" collisions, while the (e,2e) data are averaged over the full 4π solid angle. Indeed, the low-energy (e,2e + M) experiments on H_2 [11] revealed a strong orientation dependence in (e,2e + M) cross sections, with side-on collisions preferred to "end-on."

In Figs. 4(a) and 4(b) we present molecular-frame (e,2e) cross sections for the inner-valence (30 eV $\leqslant E_{Bind} <$ 50 eV) and deep-inner-valence (50 eV $\leqslant E_{Bind} <$ 70 eV) regions, respectively. The experimental results have been obtained in the following manner. First, (e,2e + M) binding-energy spectra were generated for each individual ion detector (ϕ_M). The molecular-frame (e,2e) cross sections were then obtained by summing up the number of (e,2e + M) events detected in the corresponding binding-energy regions at each ϕ_M angle. These cross sections are then plotted as a function of the angle made between $\boldsymbol{q}$ and the molecular axis. Here, the molecular axis has been drawn in the vertical direction. Note that the symmetry of our experiment allows us to present the full distribution while only performing measurements at four ϕ_M angles [7–9]. The distance of each data point from the origin represents the relative magnitude of the cross sections obtained at the corresponding ϕ_M angle.

Also included in Figs. 4(a) and 4(b) are associated PWIA calculations. The spectroscopic factors weighting the Dyson orbitals were 0.788($2\sigma_g$), 0.065($2\sigma_u$), 0.043($1\pi_u$), and 0.056($3\sigma_g$) for the inner-valence region and 0.026($2\sigma_g$), 0.031($2\sigma_u$), 0.010($1\pi_u$), and 0.010($3\sigma_g$) for the deep-inner-valence region. To make comparisons between experiment and theory, the experimental results have been globally normalized to the PWIA calculations in the inner-valence region. Last, we present in Fig. 4(c) results of the PWIA calculation for the $1\pi_u$ orbital with a spectroscopic factor of unity.

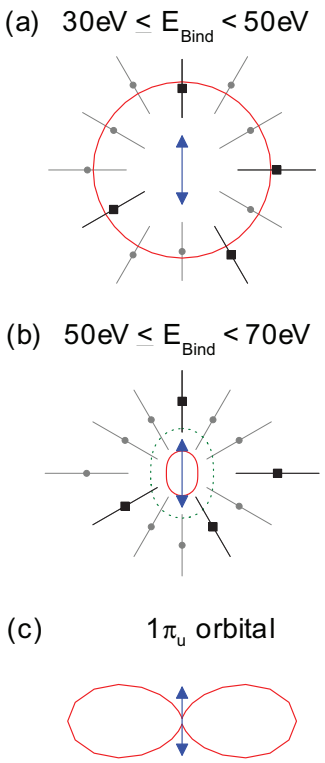

FIG. 4. (Color online) Experimental molecular-frame $(e,2e)$ cross sections (black squares: measured data points; gray dots: data points inferred from symmetry) and associated PWIA calculations (solid red line) for (a) the inner-valence and (b) deep-inner-valence regions of N_2. Also shown in (b) is the PWIA calculations scaled by a factor of 2 (dotted green line). (c) PWIA molecular-frame $(e,2e)$ cross sections for the $1\pi_u$ orbital. The direction of the N_2 molecular axis is indicated by the arrows. See text for details.

Although the statistics of the experimental data in Figs. 4(a) and 4(b) leave much to be desired, they appear to show that the angular distributions of the $(e,2e)$ cross sections are dependent upon the ionization process of interest. If these observations are real, they would indicate that while the experimental results for the inner-valence region exhibit an isotropic angular distribution, those for the deep-inner-valence region suggest potential anisotropy with a possible maximum in the direction perpendicular to the molecular axis. Also, the former observation is reproduced well by the associated PWIA calculations, but the latter is not even described in a qualitative manner. The PWIA calculations for the deep-inner-valence region exhibit substantially smaller intensity than the experiments, and they also predict maxima in the direction parallel to the molecular axis rather than perpendicular.

The agreement between experiment and PWIA for the inner-valence region can be understood in a straightforward fashion. In this region the cross section is dominated by the $2\sigma_g$ orbital, whose spatial character is highly isotropic in position space. With the orbital symmetry being invariant under the Fourier transform, the molecular-frame $(e,2e)$ cross sections are expected to be isotropic. Thus the agreement between experiment and PWIA demonstrates that the full spatial character of the N_2 $2\sigma_g$ orbital has been imaged in momentum space.

Conversely, the comparison between experiment and PWIA for the deep-inner-valence region has revealed significant issues. These issues are, within PWIA, twofold. One is the contribution from states whose intensity is missing through a limited description of the electronic structure [19], and the other is contributions from double ionization. Thus, more-sophisticated calculations would be desired to resolve the disagreement observed with the experiment, although such calculations are extremely challenging. In this respect, if we compare the experimental results for the deep-inner-valence region with PWIA calculations scaled by a factor of 2, also shown in Fig. 4(b), it appears that the theory reasonably predicts the intensity to within the experimental statistics, except in the direction perpendicular to the molecular axis. This observation suggests two important points regarding electron-impact ionization at these binding energies. First, with an assumption that the $(e,2e)$ intensity is somewhat described by ionization-excitation processes [19], such highly excited states should undergo a subsequent autoionization process to produce the two-fragment ions. Second, it is only the $1\pi_u$ orbital that gives substantial intensity in the direction perpendicular to the molecular axis, as shown in Fig. 4(c). Note that the ionization of the $3\sigma_g$ and $2\sigma_g$ orbitals is expected to produce largely isotropic molecular-frame distributions, while the $2\sigma_u$ orbital should yield a maximum in the direction along the molecular axis. As such, additional $1\pi_u$ orbital contributions may be required to resolve the disagreements noted between PWIA and molecular-frame $(e,2e)$ distributions. However, we have to leave further discussion of this issue for later experiments with improved statistics of the data. The role of double ionization and higher-order effects beyond PWIA should also be examined. Specifically, second-order contributions from the two-step mechanisms [25,26] may have to be investigated, as they have been found to significantly contribute to ionization-excitation processes of H_2 [7–9,27] and ionization-excitation and double-ionization processes of He [28–30] at large momentum transfer.

IV. CONCLUSIONS

We have presented an extension of the $(e,2e+\mathrm{M})$ technique at large momentum transfer to N_2. This has enabled an experimental observation of the spatial character of the N_2 $2\sigma_g$ orbital in momentum space. Here, the PWIA gave a good description of the $2\sigma_g$ orbital in the molecular frame. Detailed theoretical explanations are eagerly awaited to explain the disagreement observed between experiment and PWIA for the deep-inner-valence region.

ACKNOWLEDGMENTS

This research was partially supported by a Grant-in-Aid for Scientific Research (S), No. 20225001, from the Japan Society for the Promotion of Science (JSPS) and JSPS Fellows, Grant No. 20-08762. D.B.J. gratefully acknowledges JSPS for support provided by a postdoctoral fellowship.

[1] I. E. McCarthy and E. Weigold, Phys. Rep. **27**, 275 (1976).
[2] I. E. McCarthy and E. Weigold, Rep. Prog. Phys. **54**, 789 (1991).
[3] M. A. Coplan, J. H. Moore, and J. P. Doering, Rev. Mod. Phys. **66**, 985 (1994).
[4] E. Weigold and I. E. McCarthy, *Electron Momentum Spectroscopy* (Kluwer Academic, New York, 1999).
[5] V. G. Neudatchin, Yu. V. Popov, and Yu. F. Smirnov, Phys. Usp. **42**, 1017 (1999).
[6] M. Takahashi, Bull. Chem. Soc. Jpn. **82**, 751 (2009).
[7] M. Takahashi, N. Watanabe, Y. Khajuria, K. Nakayama, Y. Udagawa, and J. H. D. Eland, J. Electron Spectrosc. Relat. Phenom. **141**, 83 (2004).
[8] M. Takahashi, N. Watanabe, Y. Khajuria, Y. Udagawa, and J. H. D. Eland, Phys. Rev. Lett. **94**, 213202 (2005).
[9] M. Takahashi and Y. Udagawa, in *Nanoscale Interactions and Their Applications: Essays in Honour of Ian McCarthy*, edited by F. Wang and M. J. Brunger (Transworld Research Network, Kerala, India, 2007), Chap. 15, pp. 157–168.
[10] R. N. Zare, Mol. Photochem. **4**, 1 (1972).
[11] S. Bellm, J. Lower, E. Weigold, and D. W. Mueller, Phys. Rev. Lett. **104**, 023202 (2010).
[12] A. Senftleben, T. Pflüger, X. Ren, O. Al-Hagan, B. Najjari, D. Madison, A. Dorn, and J. Ullrich, J. Phys. B **43**, 081002 (2010).
[13] A. Senftleben, O. Al-Hagan, T. Pflüger, X. Ren, D. Madison, A. Dorn, and J. Ullrich, J. Chem. Phys. **133**, 044302 (2010).
[14] X. Ren, T. Pflüger, S. Xu, J. Colgan, M. S. Pindzola, A. Senftleben, J. Ullrich, and A. Dorn, Phys. Rev. Lett. **109**, 123202 (2012).
[15] J. Lower, J. Baxendell, and S. Bellm, in *Nanoscale Interactions and Their Applications: Essays in Honour of Ian McCarthy*, edited by F. Wang and M. J. Brunger (Transworld Research Network, Kerala, India, 2007), Chap. 9, pp. 95–106.
[16] S. Bellm, J. Lower, D. W. Mueller, and E. Weigold, J. Phys. Conf. Ser. **212**, 012005 (2010).
[17] M. Takahashi, J. P. Cave, and J. H. D. Eland, Rev. Sci. Instrum. **71**, 1337 (2000).
[18] J. H. D. Eland, M. Takahashi, and Y. Hikosaka, Faraday Discuss. **115**, 119 (2000).
[19] D. B. Jones, M. Yamazaki, N. Watanabe, and M. Takahashi, Phys. Rev. A **86**, 062707 (2012).
[20] P. Duffy, D. P. Chong, M. E. Casida, and D. R. Salahub, Phys. Rev. A **50**, 4707 (1994).
[21] M. E. Casida, Phys. Rev. A **51**, 2005 (1995).
[22] T. Aoto, K. Ito, Y. Hikosaka, A. Shibasaki, R. Hirayama, N. Yamamono, and E. Miyoshi, J. Chem. Phys. **124**, 234306 (2006).
[23] W. Eberhardt, E. W. Plummer, I.-W. Lyo, R. Carr, and W. K. Ford, Phys. Rev. Lett. **58**, 207 (1987).
[24] Y. H. Jiang, A. Rudenko, M. Kurka, K. U. Kühnel, Th. Ergler, L. Foucar, M. Schöffler, S. Schössler, T. Havermeier, M. Smolarski, K. Cole, R. Dörner, S. Düsterer, R. Treusch, M. Gensch, C. D. Schröter, R. Moshammer, and J. Ullrich, Phys. Rev. Lett. **102**, 123002 (2009).
[25] T. A. Carlson and M. O. Krause, Phys. Rev. **140**, A1057 (1965).
[26] R. J. Tweed, Z. Phys. D **23**, 309 (1992).
[27] M. Takahashi, Y. Khajuria, and Y. Udagawa, Phys. Rev. A **68**, 042710 (2003).
[28] N. Watanabe, Y. Khajuria, M. Takahashi, Y. Udagawa, P. S. Vinitsky, Yu. V. Popov, O. Chuluunbaatar, and K. A. Kouzakov, Phys. Rev. A **72**, 032705 (2005).
[29] N. Watanabe, M. Takahashi, Y. Udagawa, K. A. Kouzakov, and Yu. V. Popov, Phys. Rev. A **75**, 052701 (2007).
[30] N. Watanabe, K. A. Kouzakov, Yu. V. Popov, and M. Takahashi, Phys. Rev. A **77**, 032725 (2008).